

# Modulation of Contactless High Intensity Pulsed Electromagnetic Field Induced Electroporation and Gene Delivery Efficacy Using Various Nanoparticles

Tamara Polajžer, PhD,<sup>1</sup> Matej Kranjc, PhD,<sup>1</sup> Slavko Kralj, PhD,<sup>2,3</sup> Maja Caf, MSc,<sup>2,3</sup> Rok Romih, PhD,<sup>4</sup> Samo Hudoklin, PhD,<sup>4</sup> Vitalij Novickij, PhD,<sup>5,6</sup> and Damijan Miklavčič, PhD<sup>1</sup>

## Abstract

**Introduction:** High-intensity pulsed electromagnetic fields (HI-PEMF) can be used to trigger contactless permeabilization of the plasma membrane similar to electroporation (EP). The permeabilization efficiency and gene delivery by HI-PEMF *in vitro* are currently inferior to EP. It was suggested that the methodology can be improved with conductive gold nanoparticles (AuNPs), which are reported to amplify the induced electric field in close proximity to the cell membrane.

**Objectives:** Therefore, in this work, we have studied different NPs, which varied in material/conductivity (gold and silica), size (10–50+ nm), shape (i.e., round and rods), concentration (50–200 µg/mL), and functionalization (pegylated or not), and combined them with HI-PEMF (6.7 T × 100 pulses, 1 Hz).

**Methods:** The normal Chinese hamster ovary cell line (CHO) and the cancer human urinary bladder's transitional carcinoma cell line (T24) were used as a model. We have characterized cell membrane permeabilization using propidium iodide (PI) and the efficacy of gene delivery using pEGFP-N1.

**Results:** Larger NPs and higher NP concentrations resulted in up to a 10% increase in membrane permeability. In contrast, semispherical and rod-shaped AuNPs did not further enhance permeabilization efficiency. Gene delivery efficiency increased from 3% in control samples to 6% in the presence of 50 nm AuNPs. Overall, CHO cells were more susceptible to HI-PEMF-induced effects than T24 cells.

**Conclusions:** This study shows the potential to increase gene delivery efficacy by combining HI-PEMF treatment with conductive NPs. However, it was concluded that the HI-PEMF-induced effects are highly dependent on the cell line, NP type, and concentration and therefore require further investigation.

**Keywords:** HI-PEMF, membrane permeabilization, gene delivery, nanoparticles

## Introduction

Gene therapies in general carry the potential to tackle most critical and difficult health issues, including rapid vaccine development like that against SARS-CoV-2 and rare, debilitating hereditary diseases.<sup>1,2</sup> Recent successes in clinical studies have further increased interest in gene therapies, but bottlenecks persist, including the lack of safe and efficient methods for gene delivery. While viral vectors are a natural choice to deliver nucleic acids into the target cells, their use is limited as they have limited cargo capacity and carry major safety concerns.<sup>1,2</sup>

Electroporation is one of the most promising nonviral alternatives, which is based on the application of pulsed electric fields (PEFs) and cell plasma membrane permeabilization. During application of high-intensity PEF (pulses applied via electrodes), the permeability of the cell membrane is increased due to a transient increase in cell membrane permeability. At the same time, electric pulses facilitate movement of negatively charged nucleic acids by electrophoresis; therefore, the transfection method is known as gene electrotransfer (GET).<sup>3</sup> Success rates of electroporation and GET depend predominantly on pulse parameters,

<sup>1</sup>Faculty of Electrical Engineering, University of Ljubljana, Ljubljana, Slovenia.

<sup>2</sup>Department for Materials Synthesis, Jožef Stefan Institute, Ljubljana, Slovenia.

<sup>3</sup>Faculty of Pharmacy, University of Ljubljana, Ljubljana, Slovenia.

<sup>4</sup>Faculty of Medicine, Institute of Cell Biology, University of Ljubljana, Ljubljana, Slovenia.

<sup>5</sup>Faculty of Electronics, Institute of High Magnetic Fields, Vilnius Gediminas Technical University, Vilnius, Lithuania.

<sup>6</sup>Department of Immunology and Bioelectrochemistry, State Research Institute Centre for Innovative Medicine, Vilnius, Lithuania.

but exact mechanisms of GET are not yet fully elucidated.<sup>4</sup> GET, that is, plasmid DNA (pDNA) transfer into cells and gene expression can reach up to an 80% success rate in some cells *in vitro*.<sup>5</sup> Electroporation also allows the introduction of large DNA molecules into cells including CRISPR Cas9, thus enabling gene editing.<sup>6</sup> Electroporation has proven to be extremely useful in biomedical research. It is used in the treatment of cancer by facilitating intracellular drug accumulation in cells and thereby increasing its cytotoxicity in a treatment called electrochemotherapy, for gene therapy, DNA vaccination, and as a nonthermal soft tissue ablation method.<sup>7–9</sup>

Classical electroporation requires electrode contact with a tissue to establish an electric field in the tissues. Application of high-voltage electric pulses via electrodes induces pain and muscle contractions. In the case of invasive electrodes, the tissue is damaged, therefore increasing the risk of inflammation. Finally, the mammalian tissues are highly heterogeneous, which results in unpredictable spatial electric field distribution.<sup>10</sup> Tissue damage around the electrodes and inability to ensure the required electric field compromise the success of the whole procedure (regions of under- or over-treatment). High-intensity pulsed electromagnetic field (HI-PEMF) is a contactless method, which causes less tissue damage, does not result in pain or muscle contraction, but, at the same time, offers all the benefits of controlled molecular delivery as electroporation does.<sup>11,12</sup>

HI-PEMF-induced electroporation is based on repetitive pulsed high magnetic fields in the range of a few Teslas. HI-PEMF was shown to increase membrane permeabilization similar to electroporation and can thus be used to facilitate transmembrane molecular transport<sup>11–14</sup> and the introduction of large molecules such as pDNA into target cells. HI-PEMF has also been used for the successful delivery of siRNA and plasmid encoding green fluorescent protein (GFP) protein *in vivo*<sup>15,16</sup> and *in vitro*.<sup>17</sup> Nevertheless, while membrane permeabilization and GET can be achieved using HI-PEMF, its efficacy is inferior when compared to PEF. The improvement in HI-PEMF treatment efficacy is therefore of great interest, and one such option represents the introduction of nanoparticles (NPs). The interaction between NPs and electromagnetic fields has been demonstrated previously. For example, barium-hexaferrite nanoplatelets were activated by low-frequency alternating magnetic fields to disrupt the lipid membrane,<sup>18</sup> and gold NPs (AuNPs) were shown to be electrophoretically driven close to the cell plasma membrane by PEFs.<sup>19</sup> Interestingly, it has been suggested theoretically and demonstrated experimentally that NPs can facilitate electroporation: GET, drug delivery/electrochemotherapy, and even extent the area of tissue being ablated by irreversible electroporation.<sup>20–24</sup> NPs used in these experiments were mainly carbon nanotubes and conductive/metal NPs such as gold and platinum NPs. The underlying assumption is that conductive NPs locally amplify electric field, and thus, if close to the plasma membrane, allow its electroporation at lower electric fields. It has been shown that the presence of AuNPs can improve the membrane permeabilization efficacy in the HI-PEMF treatment.<sup>16</sup>

To investigate the influence of NPs' properties on the HI-PEMF treatment further with the aim to improve membrane permeabilization and gene delivery, we used different NPs, which varied in size, shape, functionalization, and material.

We determined membrane permeabilization and gene delivery using the combination of HI-PEMF treatment and different NPs on two different cell lines *in vitro*.

## Materials and Methods

### Nanoparticles

**Chemicals.** Hydrogen tetrachloroaurate trihydrate (HAuCl<sub>4</sub>·3H<sub>2</sub>O, 99.99%) and sodium hydroxide (NaOH, 98%) were obtained from Alfa Aesar. Silver nitrate (≥99.8%), citric acid monohydrate (99.5–100.5%), bis(*p*-sulfonatophenyl)phenylphosphine (97%), and L-(+)-ascorbic acid (99.5–100.5%) were purchased from Sigma-Aldrich. Sodium borohydride (NaBH<sub>4</sub>, 98+%) was supplied by Acros Organics. Sodium chloride (NaCl, ≥99.5%) was obtained from Fisher Scientific. Surfactants and stabilizers, including hexadecyltrimethylammonium bromide (CTAB) and Tween 80, were purchased from VWR and Fisher Bioreagents, respectively. O-(2-mercaptoethyl)-O'-methylpolyethylene glycol (MeO-PEG-SH, MW 2000) was also obtained from Sigma-Aldrich. All chemicals were used as received, without further purification.

**Synthesis and PEGylation of gold nanorods.** Gold nanorods (AuNRs) were synthesized using a seed-mediated growth method adapted from Nikoobakht and El-Sayed.<sup>25</sup> The synthesis consisted of two main stages: seed preparation and nanorod growth.

**Seed preparation.** A 5 mL solution of hydrogen tetrachloroaurate(III) trihydrate (0.00050 M) was freshly prepared and cooled prior to use. It was then mixed with 5 mL of 0.2 M CTAB under vigorous stirring. Immediately after, 0.6 mL of ice-cold sodium borohydride (0.010 M) was rapidly added to the mixture. A prompt color change from yellow to brown indicated the formation of gold seed particles. The mixture was stirred for an additional 2 min and subsequently incubated in the dark at 30°C for 4 h to allow for seed maturation.

**Growth solution preparation and nanorod formation.** Prior to growth, all reagents were equilibrated in a water bath at 30°C for 1 h. The following stock solutions were prepared: 127 mL of 0.001 M HAuCl<sub>4</sub>·3H<sub>2</sub>O, 127 mL of 0.2 M CTAB, 3.83 mL of 0.0040 M silver nitrate (AgNO<sub>3</sub>), and 1.786 mL of 0.0788 M L-ascorbic acid. To prepare the growth solution, silver nitrate, CTAB, and the gold precursor were combined under vigorous stirring. The addition of ascorbic acid triggered a rapid color change from yellow to colorless, indicating the reduction of gold ions to Au<sup>0</sup>.

Immediately thereafter, 0.306 mL of the previously prepared seed solution was introduced into the growth mixture, followed by gentle stirring for 30 s. The reaction was then left undisturbed to proceed overnight at 30°C in the dark.

**Purification.** To remove excess CTAB, the resulting AuNRs were purified by two cycles of ultracentrifugation at 20,000g for 20 min, followed by resuspension in distilled water.

**Functionalization with PEG.** AuNRs were functionalized with polyethylene glycol (PEG) following the method

described by Liu et al.<sup>26</sup> with slight modifications. Briefly, separate stock solutions were prepared: 2 vol% Tween 80, 25  $\mu\text{L}$  of 0.1 M bis(*p*-sulfonatophenyl)phenylphosphine, 63  $\mu\text{L}$  of 1.6 mM MeO-PEG-SH, and 250  $\mu\text{L}$  of 2 M sodium chloride (NaCl). These compounds were mixed and stirred for 1 min prior to the addition of the AuNR suspension. The mixture was then gently shaken overnight to allow for complete PEGylation. Following the reaction, the PEG-functionalized AuNRs (AuNRs-PEG) were purified by two cycles of washing with distilled water to remove excess reagents.

**Synthesis of quasi-spherical 10 nm AuNPs.** The synthesis of 10 nm AuNPs (10-AuNPs) was adapted from the protocol reported by Ojea-Jiménez et al.<sup>27</sup> Briefly, 102 mL of 2.45 mM sodium hydroxide and 2.1 mL of 0.34 M sodium citrate were mixed in a round-bottom flask equipped with a reflux condenser and heated in an oil bath until boiling. Once the solution reached boiling temperature, 2 mL of 0.066 M hydrogen tetrachloroaurate trihydrate was rapidly added under vigorous stirring. The solution immediately turned black, followed by a gradual shift to a deep wine-red color, indicating the formation of AuNPs. Upon completion of the reaction, the colloidal suspension was rapidly cooled to room temperature using an ice bath. The resulting 10-AuNPs were then washed with distilled water to remove residual reagents.

**Synthesis of quasi-spherical ~50 nm AuNPs (50-AuNPs).** AuNPs with an average diameter close to 50 nm (50-AuNPs) were synthesized using a multi-step seed-mediated growth approach, adapted from the method described by Bastús et al.<sup>28</sup> Stock aqueous solutions of sodium citrate (2.2 mM and 60 mM) and hydrogen tetrachloroaurate (25 mM) were freshly prepared prior to synthesis.

**Seed preparation.** To produce gold seed particles, 37.5 mL of 2.2 mM sodium citrate solution was heated in a 100 mL round-bottom flask equipped with a reflux condenser and immersed in an oil bath until boiling. Upon reaching the boiling point, 0.25 mL of 25 mM HAuCl<sub>4</sub> was rapidly injected under vigorous stirring. A light pink coloration appeared within 1 min, indicating the formation of seed NPs. The suspension was then removed from heat and allowed to cool to 90°C at room temperature.

**First growth step.** Once cooled, the seed solution was returned to the oil bath and maintained at 90°C with a reduced stirring speed of 600 rpm. To initiate growth, 0.25 mL of HAuCl<sub>4</sub> solution was added to the reaction, followed by two additional 0.25 mL aliquots, each added at 10 min intervals.

**Subsequent growth cycles.** In parallel, a secondary growth solution was prepared by heating 13.25 mL of distilled water and 0.5 mL of 60 mM sodium citrate to 90°C. Once the target temperature was reached, 13.75 mL of the previously prepared NP suspension was added to this solution. This was followed by three sequential additions of 0.25 mL HAuCl<sub>4</sub>, each spaced 10 min apart. The dilution-growth cycle was repeated four times to incrementally increase particle size.

**Purification.** Following the final growth step, the resulting AuNPs (50-AuNPs) were washed with distilled water to remove excess citrate and other residual reagents.

**PEGylation of AuNPs (10-AuNPs-PEG and 50-AuNPs-PEG).** Both 10 nm and 50 nm AuNPs were functionalized with PEG using the same protocol. Each NP suspension was added dropwise into a vigorously stirred solution of 0.125 mM MeO-PEG-SH in a total volume of 20 mL. The mixture was allowed to react overnight at room temperature to ensure complete surface coverage. The following day, PEGylated NPs (10-AuNPs-PEG and 50-AuNPs-PEG) were purified by a single washing step with distilled water to remove unbound PEG molecules.

**Synthesis of silica NPs.** Silica NPs (SiO<sub>2</sub>-NPs) were synthesized using a modified Stöber method.<sup>29</sup> In a typical procedure, 50 mL of deionized water, 4.5 mL of aqueous ammonia, and 50 mL of a 0.27 M tetraethyl orthosilicate solution were combined in a reaction flask and stirred continuously overnight at room temperature. Upon completion of the synthesis, the resulting SiO<sub>2</sub>-NPs were collected and purified by three successive washing steps with distilled water.

**Characterization of NPs.** Transmission electron microscopy (TEM) analysis was performed using a JEOL 2100 microscope equipped with energy-dispersive X-ray spectroscopy (JED 2300 EDS). For all NP types, TEM grids were prepared by drop-casting ~20  $\mu\text{L}$  of the diluted suspension onto carbon-coated copper grids, followed by air drying at room temperature. Particle size distributions were determined using ImageJ software based on the manual analysis of a statistically significant dataset ( $N = 500$  particles).

Zeta potential measurements were conducted using a Lite-sizer 500 instrument (Anton Paar, Austria). NP suspensions were diluted to a final concentration of 250  $\mu\text{g}/\text{mL}$ . Zeta potential measurements were performed in distilled water (pH was 7.2–7.4) as well as in both types of cellular media containing proteins (HAM medium: HAM F-12 growth medium supplemented with 10% fetal bovine serum [FBS]) and DMEM medium: A-DMEM:F12 growth medium supplemented with 5% FBS), using disposable cuvettes for analysis under standard measurement conditions.

### Cells

The CHO was purchased from the European Collection of Authenticated Cell Cultures. Cells were grown in HAM F-12 growth medium (PAA, Austria) supplemented with 10% FBS (Sigma-Aldrich, USA), L-glutamine (0.5% for CHO, 2% for H9c2) (StemCell, Canada), penicillin/streptomycin (PAA, Austria), and 0.1% gentamycin (Sigma-Aldrich, USA) in an incubator at 37°C with controlled atmosphere (CHO at 5% CO<sub>2</sub>, H9c2 at 10% CO<sub>2</sub>). The human urinary bladder's transitional carcinoma cell line (T24) was purchased from the American Type Culture Collection. Cells were grown in A-DMEM:F12 growth medium (Gibco, Thermo Fisher Scientific, USA), mixed 1:1, and supplemented with 5% FBS (Gibco) and 4 mM Glutamax (Gibco). T24 cells were grown in an incubator at 37°C with a controlled atmosphere (5% CO<sub>2</sub>).

Growth medium was removed, and the trypsin-EDTA (PAA, Austria) was added to detach cells. After 3 min, fresh medium was added to inactivate trypsin. Cell suspension was then centrifuged at 180 g for 5 min, the supernatant was removed, and the cells were resuspended in cell growth media to obtain different concentrations of NPs (0, 50, 100, or 200  $\mu\text{g}/\text{mL}$ ) and  $1 \times 10^6$  cells/mL or, in the case of GET,  $2 \times 10^6$  cells/mL density. Cell suspension was incubated at 4°C for 15 min, and afterward HI-PEMF treatment was delivered.

#### HI-PEMF treatment

HI-PEMF was applied with the pulse generator previously described.<sup>13</sup> As an applicator, a solenoid coil was used (11.8  $\mu\text{H}$ ), wound from enamel-insulated copper wire (6 layers  $\times$  8 windings, wire diameter: 0.5 mm, and effective radius = 2 mm). The magnetic field was 6.7 T in the middle of the coil, and the induced electric field was up to 20 V/cm near the coil windings, declining toward 0 at the geometric center of the coil. The HI-PEMF was generated using a half-sinusoidal pulse with a peak voltage of 3 kV and a peak electric current of 1 kA.<sup>13</sup> A total of 100 pulses were used, delivered at a repetition frequency of 1 Hz. As PEMF application was performed immediately after filling the tube with the cell suspension, and because each PEMF pulse caused slight coil vibrations, we assumed that no significant cell sedimentation occurred during the PEMF exposure because each PEMF pulse caused slight coil vibrations.

#### Permeabilization assay

Prior to HI-PEMF treatment, CHO and T24 cells were mixed with PI (Life Technologies) to a final concentration of 100  $\mu\text{g}/\text{mL}$ . Immediately after the treatment, 40  $\mu\text{L}$  of cell suspension was transferred to a 0.2 PCR tube (ABgene: Thermo Fisher Scientific, Waltham, MA, USA). Then, 3 min after the treatment, cell suspension was removed from the PCR tube, and the uptake of PI in the cells was analyzed by the flow cytometer (Attune NxT; Life Technologies, Carlsbad, CA, USA) using a 488 nm blue laser and a 574/26 nm band-pass filter. The analysis of 10,000 events was performed by Attune NxT software. On the dot plots of forward scatter and side scatter, the debris and clusters were excluded from the analysis. Fluorescence intensity histograms were used to determine the percentage of PI-permeabilized cells. Gating was set according to the sham control (0 V, without NPs). The measurements for each data point were repeated three times.

#### GET assay

GET was evaluated with plasmid pEGFP-N1 (Clontech Laboratories Inc., Mountain View, CA, USA) encoding GFP under the control of the CMV promoter in the size of 4.7 kb. pDNA was amplified using *Escherichia coli*, isolated with the HiSpeed Plasmid Maxi Kit (Qiagen, Hilden, Germany), and plasmid concentration was spectrophotometrically determined at 260 nm.

Prior to HI-PEMF treatment, CHO cells were mixed with the plasmid to obtain a concentration of plasmid at 100  $\mu\text{g}/\text{mL}$ . Immediately after the treatment, 40  $\mu\text{L}$  of cell suspension with plasmid was transferred to a 0.2 PCR tube, and after the treatment, 10  $\mu\text{L}$  of FBS was added to the cells and incubated

for another 5 min at 37°C. Afterward, cells were diluted in fresh growth medium, and the sample was split for two following analyses: percentage of GFP-positive cells and viability.

**Detection of transfected cells.** To determine the percentage of GFP-positive cells, cells were seeded in growth medium into a 24-well plate (Techno Plastic Products AG, Trasadingen, Switzerland) for 24 h at 37°C, 5% CO<sub>2</sub>. Afterward, cells were harvested and resuspended in 150  $\mu\text{L}$  of phosphate buffer saline (1 $\times$  PBS) and analyzed using an Attune NxT flow cytometer (Thermo Fisher Scientific, Waltham, MA, USA) with a blue laser at 488 nm and a 530/30 nm band pass filter. For every sample, 10,000 events were recorded. Fluorescence intensity histograms were used to determine the percentage of GFP-positive cells.

**Viability.** For survival analysis, cells were diluted in fresh growth medium, and  $2 \times 10^4$  cells were transferred to a 96-well plate (Techno Plastic Products AG, Trasadingen, Switzerland) and incubated at 37°C for 24 h. According to manufacturer's instructions (CellTiter 96 AQueous One Solution Cell Proliferation Assay, Promega, USA), 20  $\mu\text{L}$  of MTS tetrazolium compound was added to the samples, and after 2 h, the absorbance of formazan (reduced MTS tetrazolium compound) was measured with a spectrofluorometer (Tecan Infinite M200, Tecan, Austria) at 490 nm. The percentage of viable cells was obtained by the normalization of sample absorbance to the absorbance of the control (0 V) with the same NP type and concentration.

Overall, GET was calculated by multiplying the % of GFP-positive cells and survival after GET.

#### Statistical analysis

All experiments except TEM were repeated at least three times. The results are shown as mean  $\pm$  SD. Statistical analysis was performed using SigmaPlot 11.0 (Systat Software, USA). Statistically significant differences ( $*p < 0.05$ ) were determined by the one-way analysis of variance (ANOVA) test and the Holm–Sidak post hoc test.

## Results

#### Characterization of NPs

The effect of NPs on the efficiency of HI-PEMF-induced electroporation was investigated using a variety of conductive AuNPs differing in shape, size, and surface functionalization, as well as nonconductive SiO<sub>2</sub>-NPs. The physicochemical characteristics of all NP types are summarized in Table 1. TEM analysis confirmed that the smaller AuNPs (10-AuNPs) exhibited a narrow size distribution, with an average diameter of  $12.0 \pm 1.1$  nm (Fig. 1). Dynamic light scattering (DLS) measurements indicated no detectable aggregation upon mixing the NPs with the different media used, yielding mean hydrodynamic sizes of  $43.8 \pm 0.4$  nm,  $75.7 \pm 3.7$  nm, and  $78.3 \pm 0.8$  nm in water, DMEM, and HAM media, respectively (Table 2).

For experimental studies, either citrate-stabilized (carboxyl-terminated surface) or PEG-functionalized (methoxy-terminated surface) AuNPs were used. Zeta potential measurements revealed values of  $-11.6 \pm 0.3$  mV for citrate-

TABLE 1. CHARACTERISTICS OF THE SYNTHESIZED NANOPARTICLES USED IN OUR STUDY

Nanoparticles	Material	Shape	Size (nm) <sup>a</sup>	Surface
50-AuNPs	Gold	Quasi-spherical	57 ± 7	COOH
10-AuNPs	Gold	Quasi-spherical	12 ± 1	COOH
50-AuNPs-PEG	Gold	Quasi-spherical	57 ± 7	PEG
10-AuNPs-PEG	Gold	Quasi-spherical	12 ± 1	PEG
AuNRs-PEG	Gold	Elongated	63 ± 4 length 17 ± 2 diam	PEG
SiO <sub>2</sub> -NPs	Silica	Spherical	54 ± 6	-OH

<sup>a</sup>Size is determined by TEM image analysis.

AuNPs, gold nanoparticles; PEG, polyethylene glycol; TEM, transmission electron microscopy.

functionalized and  $-5.5 \pm 1.5$  mV for PEG-functionalized NPs (Table 3). These changes in surface potential might affect the interaction of NPs and cell membranes. However, surface charge is likely screened from salts and other components present in the electroporation buffer, which reduced the absolute value of zeta potential under experimental conditions. DLS measurements also demonstrated an absence of aggregation of the functionalized NPs in both HAM and DMEM (Table 2).

Larger AuNPs (50-AuNPs) with an average diameter of  $56.9 \pm 7.0$  nm (Fig. 2) were also synthesized, featuring the same surface functional groups—carboxyl (citrate-stabilized) or methoxy (PEGylated)—as the smaller particles. Zeta potential measurements indicated values of  $-9.7 \pm 0.5$  mV for citrate-functionalized and  $-3.3 \pm 0.7$  mV for PEG-functionalized formulations (Table 3). DLS measurements also showed good colloidal stability of both types of NPs in HAM and DMEM media (Table 2).

AuNRs were synthesized with an average diameter of  $17.1 \pm 1.8$  nm and a length of  $63.0 \pm 4.4$  nm, yielding an aspect ratio of  $\sim 4.3$ , to investigate the influence of NP shape and size. Representative TEM images and corresponding size distribution histograms are shown in Figure 3. The nanorods were synthesized in the presence of cetyltrimethylammonium bromide (CTAB), a surfactant known for its cytotoxicity. To enhance biocompatibility, the CTAB was removed by intense and repeatable washings, while remaining traces were replaced with a PEG coating using a protocol similar to that applied for quasi-spherical NPs. The resulting zeta potential values were comparable to the values

measured for the other types of PEGylated NPs included in our study.

To evaluate whether the presence of NPs alone affects cells, nonconductive SiO<sub>2</sub>-NPs ( $53.6 \pm 6.1$  nm; Fig. 4) were synthesized as a control.

#### Effect of NPs on membrane permeabilization

The influence of NPs (200  $\mu\text{g}/\text{mL}$ ) was first evaluated on membrane permeabilization efficacy, where intracellular PI accumulation was used as a marker of successfully permeabilized membrane (Fig. 5). In the absence of NPs, HI-PEMF treatment causes  $\sim 20\%$  of cell permeability in CHO cells compared to no treatment (control). However, when NPs were added, the permeabilization efficacy of HI-PEMF treatment was affected (Fig. 5A). When 10-AuNPs and 50-AuNPs were used, membrane permeability increased to 25% for 10-AuNPs and 30% for 50-AuNPs, making the permeabilization efficacy higher. Also, while there was a tendency of size dependence (i.e., larger 50-AuNPs caused a higher increase in permeability than smaller 10-AuNPs), the differences were not statistically significant ( $p < 0.05$ ).

Interestingly, when the PEG-functionalized AuNPs were used (10-AuNPs-PEG and 50-AuNPs-PEG), a statistically significant smaller permeabilization efficacy was observed (vs. HI-PEMF without NPs). Similar trends were observed with different shapes (i.e., rods AuNRs-PEG) or even with different materials, such as nonconductive control SiO<sub>2</sub>-NPs (Fig. 5A). Surprisingly, NP did not increase membrane

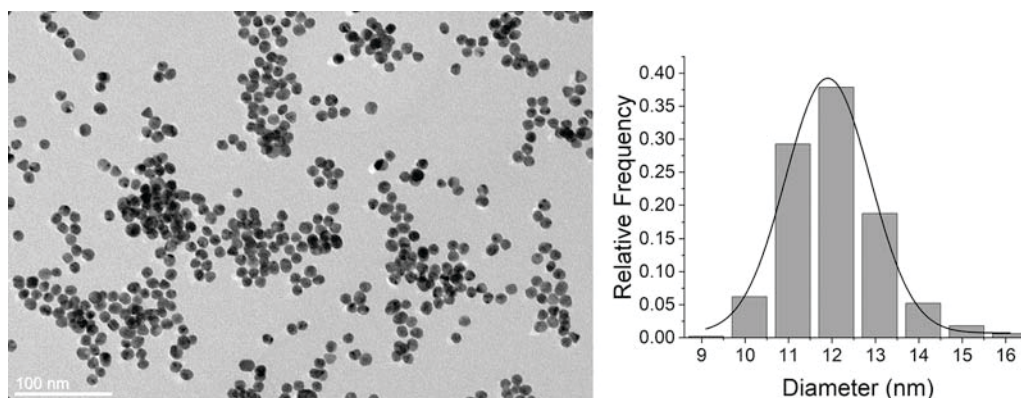


**FIG. 1.** TEM image of 10-AuNPs (left) and corresponding particle size distribution histogram based on TEM analysis (right). 10-AuNPs, 10 nm gold nanoparticles; TEM, transmission electron microscopy.

TABLE 2. DYNAMIC LIGHT SCATTERING CHARACTERIZATION OF VARIOUS NANOPARTICLES IN WATER AND TWO DIFFERENT CELLULAR MEDIA USED

Nanoparticles	Dispersing solution	Mean hydrodynamic size (nm)
10-AuNPs	Distilled water	43.8 ± 0.4
10-AuNPs-PEG	Distilled water	52.3 ± 1.1
50-AuNPs	Distilled water	64.1 ± 1.0
50-AuNPs-PEG	Distilled water	75.9 ± 1.9
SiO <sub>2</sub> -NPs	Distilled water	104.4 ± 3.7
10-AuNPs	DMEM	75.7 ± 3.7
10-AuNPs-PEG	DMEM	75.5 ± 2.6
50-AuNPs	DMEM	90.4 ± 3.2
50-AuNPs-PEG	DMEM	76.4 ± 0.1
SiO <sub>2</sub> -NPs	DMEM	222.3 ± 9.1
10-AuNPs	HAM	78.3 ± 0.8
10-AuNPs-PEG	HAM	85.4 ± 3.7
50-AuNPs	HAM	88.9 ± 3.0
50-AuNPs-PEG	HAM	76.5 ± 2.0
SiO <sub>2</sub> -NPs	HAM	491.8 ± 77.5

permeability in T24 cells regardless of the NPs' type and properties (Fig. 5B).

#### Effect of NPs on GET

As only the CHO cell line resulted in increased membrane permeabilization by NPs, only CHO cells were used in GET experiments. Since 50-AuNPs caused the highest increase in membrane permeability in CHO cells, the same NPs were used for GET experiments (Fig. 6). In addition to the no NPs (0 µg/mL) also 50, 100, and 200 µg/mL of 50-AuNPs were also used to investigate if the effect is NP concentration-dependent. For each concentration of 50-AuNPs in addition to HI-PEMF treatment, two controls were used: CTRL1—control without the plasmid and without the treatment (0 V) and CTRL2—control with the plasmid and without the treatment (0 V). This showed that the presence of plasmid and/or NPs by itself, that is, without the HI-PEMF treatment, was not achieving gene delivery.

When the lowest concentration of NPs (50 µg/mL) was used, results showed a slight (2.9%), yet statistically significant ( $p < 0.05$ ), increase in gene delivery efficacy compared to HI-PEMF treatment without the presence of NPs (Fig. 6A). With the increase in NP concentration, there was a declining tendency in gene delivery efficacy. The 50 µg/mL concentration was optimal within the studied range of concentrations. It should be noted that none of the treatments used in the study affected cell viability (Fig. 6B).

#### Discussion

The HI-PEMF-induced electroporation is a noninvasive, contactless method for drug and nucleic acid delivery into cells that may offer advantages over traditional GET, which relies on electroporation with direct-contact electrodes. Potentially, HI-PEMF offers a technological platform to trigger painless and noninvasive electroporation, mitigating adverse effects of classical electroporation. However, since HI-PEMF is a relatively new technology with a limited number of *in vitro* studies, there remains a lack of understanding of the electromagnetic, biological, biochemical, and biophysical mechanisms underlying its effects—knowledge that is essential for further development and optimization of this treatment approach.

First, it has been previously reported that the presence of AuNPs increases cell membrane permeability in HI-PEMF treatment, yet this efficacy depends on NP properties. Comparison of permeability curves performed with 5 and 20 nm AuNPs (concentrations were 10, 25, and 50 µg/mL) showed that larger and more concentrated NPs resulted in better HI-PEMF treatment efficacy, that is, higher cell membrane permeability.<sup>16</sup> Later, we reported that HI-PEMF can be used for a successfully facilitated gene delivery.<sup>17</sup> However, compared to traditional electroporation (around 60%), gene delivery efficiency was considerably lower in HI-PEMF (around 3%). This was attributed to a much lower (at least 80 times lower) and nonhomogeneously distributed electric field induced by HI-PEMF. Regardless of the low numbers, this was the first successful gene transfer into cells and GFP expression by HI-PEMF *in vitro*.<sup>17</sup> Based on the studies that HI-PEMF treatment can be improved by the addition of NPs and that successful GET can be achieved with the HI-PEMF treatment, a combination of HI-PEMF with NPs was suggested in this study.

In this work, we have studied changes in cell plasma membrane permeability when different NPs were used in combination with the HI-PEMF treatment. This study included six types of NPs, each differing by a single physicochemical property. This allowed us to isolate and evaluate the contribution of individual NP characteristics to HI-PEMF treatment efficacy. Comparisons between NP groups can be structured as size (50 nm vs. 10 nm), PEGylation (PEGylated NPs vs. non-PEGylated NPs), shape (semispherical vs. rods), and material conductivity (gold vs. silica). According to our results, HI-PEMF treatment, in the presence of NPs, affects cell membrane of different cell lines differently. As in this work, the CHO cells were less susceptible to HI-PEMF compared to T24 cells (Fig. 5). Interestingly, we could observe a NPs-specific response in the CHO cells—that is, nonfunctionalized

TABLE 3. ZETA POTENTIAL VALUES OF VARIOUS NANOPARTICLES IN WATER AND TWO DIFFERENT CELLULAR MEDIA USED

Nanoparticles	Zeta potential value in water	Zeta potential value in HAM	Zeta potential value in DMEM
50-AuNPs	-41.2 ± 5.7 mV	-9.7 ± 0.5 mV	-10 ± 0.4 mV
10-AuNPs	-15.9 ± 2.2 mV	-11.6 ± 0.3 mV	-11.3 ± 0.2 mV
50-AuNPs-PEG	-41.2 ± 5.7 mV	-3.3 ± 0.7 mV	-2.4 ± 0.2 mV
10-AuNPs-PEG	-23.5 ± 1.7 mV	-5.5 ± 1.5 mV	-6.4 ± 1.3 mV
AuNRs-PEG	-21.6 ± 1.6 mV	-4.2 ± 0.7 mV	-3.6 ± 0.3 mV
SiO <sub>2</sub> -NPs	-47 ± 0.6 mV	-10.9 ± 0.6 mV	-0.2 ± 0.1 mV

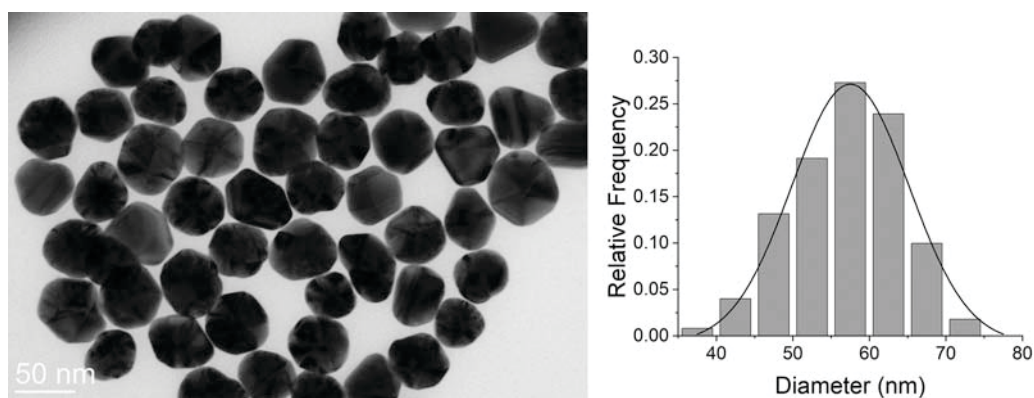


**FIG. 2.** TEM image of 50-AuNPs (left) and corresponding particle size distribution histogram (right), based on TEM analysis. 50-AuNPs, 50 nm gold nanoparticles.

(non-PEGylated) AuNPs demonstrated an increase in permeabilization, while other NP types (PEGylated) induced a smaller statistically significant effect. While smaller 10-AuNPs resulted in a lower efficacy than 50-AuNPs, this difference was not statistically significant. The response of nonfunctionalized AuNPs is in agreement with our previous study.<sup>16</sup>

Comparison of the PEGylated version of NPs versus the non-PEGylated version of NPs (10-AuNPs-PEG vs. 10-AuNPs and 50-AuNPs-PEG vs. 50-AuNPs) showed that PEGylation reduces NPs efficacy in HI-PEMF treatment. Furthermore, comparison of NP shapes (semispherical 50-AuNPs-PEG vs. rod-like AuNRs-PEG) revealed no efficacy in HI-PEMF treatment. Similar behavior was observed when different material compositions of NPs were studied (50-AuNPs vs. SiO<sub>2</sub>-NPs) (Fig. 5A). Surprisingly, in the case of the T24 cell line, none of the NP types involved in the study induced statistically significant improvement in cell membrane permeabilization, and no differences in efficacy were detected, which suggests that NP efficacy is cell-type dependent (Fig. 5B). The cell lines used come from different species, tissues, and health statuses (cancerous/noncancerous), which can cause different behavior.<sup>30</sup>

The reason for the very similar efficacy of different NP types in the HI-PEMF treatment (Fig. 5) could be in the dispersing medium, where citrate buffer was replaced with cell media containing proteins. Electroporation efficiency—probably also HI-PEMF—is strongly influenced by the

composition of the electroporation buffer.<sup>31,32</sup> However, since our HI-PEMF experiments were performed directly in complete culture media, replacing citrate buffer with cell culture medium ensured that the observed effects reflected only the contribution of NP presence, without introducing additional citrate ions into the experimental system.<sup>17,33</sup> Furthermore, the citrate surface coverage of AuNPs is typically reported to be between  $\sim 1$  and 5 molecules nm<sup>-2</sup>.<sup>34,35</sup> Assuming the upper limit of 5 molecules nm<sup>-2</sup>, complete desorption from the NP surface (density of gold is  $\sim 19.3$  g/mL—relatively low specific surface area) would correspond to a maximum free citrate concentration of  $\sim 52$   $\mu$ M for 10 nm AuNPs (lower citrate concentration for larger NPs; at the highest tested NP concentration of 200  $\mu$ g/mL) in our experimental conditions. Importantly, literature indicates that biological effects of extracellular citrate—such as changes in viability, membrane permeability, or calcium homeostasis—occur only at millimolar concentrations (1–20 mM). For instance, Wu et al.<sup>36</sup> reported cytotoxic effects at  $\sim 5$  mM citrate, Caiazza et al.<sup>37</sup> observed metabolic alterations at 10–20 mM, and von Schirnding et al.<sup>38</sup> described calcium-citrate-induced cell death only at high millimolar levels. Physiological extracellular citrate concentrations are typically around 100–150  $\mu$ M,<sup>39</sup> meaning that our estimated 52  $\mu$ M—if released completely from the surface of NPs—would still remain well below physiologically relevant levels. Collectively, these data strongly indicate that any potential contribution from free citrate ions would be negligible in our experimental system, and the

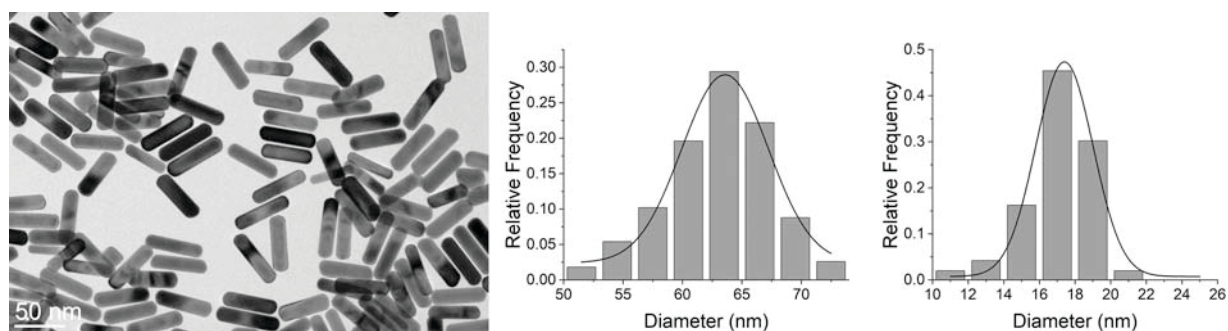


**FIG. 3.** TEM image of gold nanorods (left), with length distribution shown in the center and width distribution on the right.

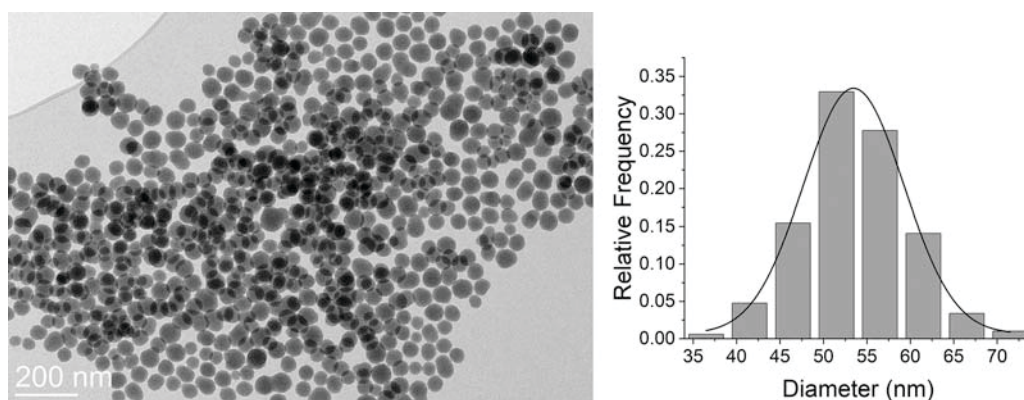


**FIG. 4.** TEM image of spherical silica nanoparticles (left) and corresponding particle size distribution histogram (right), based on TEM analysis.

observed responses can be attributed to the AuNPs themselves.

Furthermore, PEG-functionalized NPs provide steric stabilization, as the PEG chains (2 kDa) sterically repel NPs from each other and from the cell membrane. The PEG chains introduce steric hindrance, creating a physical barrier that prevents close interaction between the NPs and the cell membrane.<sup>40</sup> This steric repulsion likely limits the ability of PEG-functionalized NPs to approach or adsorb onto the membrane surface, thereby reducing their potential to locally enhance the electric field during electroporation and HI-PEMF treatment. The zeta potential values revealed that proteins from media form a protein corona even in the case of PEGylated NPs, as the absolute values of zeta potential were decreased (Table 3). This somehow shows that differences in zeta potential arising from initial functionalization (PEG vs. citrate) were effectively masked by adsorbed proteins. Therefore, consistent with this, our experiments with quasi-spherical PEG- and COOH-functionalized AuNPs exhibited similar behavior across all measured endpoints.

Based on membrane permeability results, only CHO resulted in increased permeability (Fig. 5). Therefore, HI-PEMF for gene delivery was tested only on CHO cells. This was performed with NPs that resulted in the highest efficacy of treatment, that is, 50-AuNPs. As expected, gene delivery efficacy increased from 3% to 5.9%, which is still relatively low in absolute value, yet the increase was almost 100% (Fig. 6). Interestingly, the largest percentage of GFP-positive cells was at the lowest concentration of NPs. The percentage of GFP-positive cells dropped with an increase in NP concentration. Cell viability was unaffected even at the highest NP concentration, suggesting NPs are not cytotoxic. The decrease in efficiency at higher NP concentrations may be due to interference with pDNA or modulation of cellular uptake processes such as endocytosis; however, we do not have direct evidence for this. In traditional electroporation, small molecules are believed to enter cells directly via electrophoretic transport, whereas larger molecules tend to accumulate at the membrane and are internalized via endocytosis.<sup>4,41,42</sup> Also, our previous study indicates that HI-PEMF-mediated gene

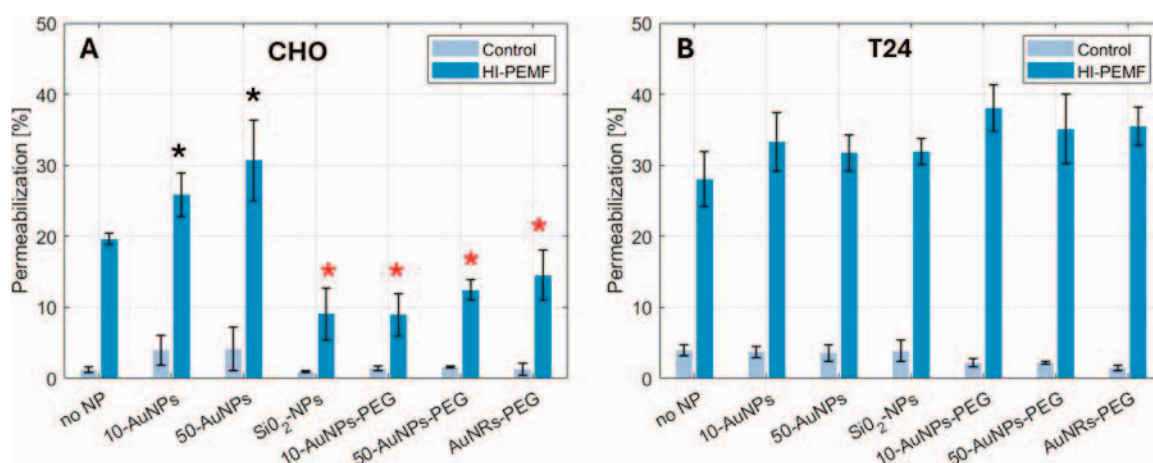


**FIG. 5.** Membrane permeabilization after HI-PEMF treatment on (A) CHO and (B) T24 cells in the presence of nanoparticles. Results are presented as a mean value, and bars represent standard deviation. All HI-PEMF treatments were statistically significantly higher than without HI-PEMF treatment (control). A black asterisk (\*) marks a statistically significant increase in HI-PEMF treatment, and a red asterisk (\*) marks a statistically significant decrease in HI-PEMF treatment compared to HI-PEMF treatment without NPs. CHO, Chinese hamster ovary cell line; HI-PEMF, high-intensity pulsed electromagnetic fields; NPs, nanoparticles; T24, human urinary bladder's transitional carcinoma cell line.

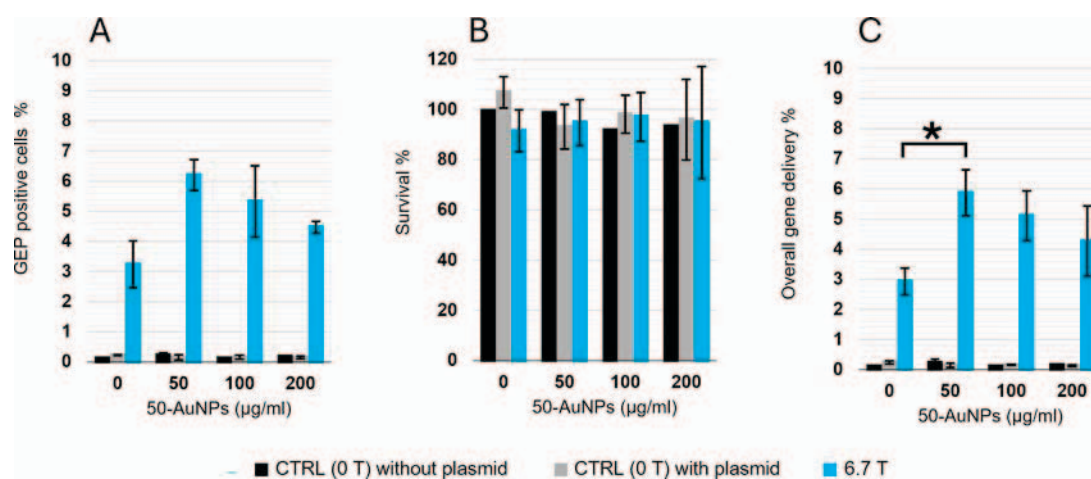


**FIG. 6.** Gene delivery after HI-PEMF treatment on CHO cells with 50-AuNPs. (A) GFP-positive cells, (B) survival, and (C) overall GET. Results are presented as a mean value, and bars represent standard deviation. Asterisk (\*) marks a statistically significant decrease in overall GET after HI-PEMF treatment compared to HI-PEMF treatment without NPs (0 µg/mL). GET, gene electrotransfer; GFP, green fluorescent protein.

delivery occurs primarily through endocytic pathways.<sup>17</sup> We have also shown that HI-PEMF exposure can promote the formation of DNA–membrane complexes, which is a known prerequisite for endocytic uptake of large biomolecules.<sup>17</sup> We emphasize that the suggested mechanisms for the reduced efficiency at higher NP concentrations are speculative, as the exact mechanism of GET is not yet fully understood.<sup>3,43</sup> Testing these hypotheses directly, for example, through zeta potential measurements or microscopy to observe nanoparticle–DNA–cell interactions, would require a separate study and was beyond the scope of the current work.

In conclusion, our study has shown the potential to enhance gene delivery efficacy using HI-PEMF treatment and NPs. Nevertheless, it was observed that HI-PEMF-induced effects are dependent on the cell line, NP type, and concentration and therefore require further optimization, especially for gene transfer in cancer cells.

#### Authors' Contributions

T.P. and M.K.: Data curation, formal analysis, investigation, methodology, visualization, writing—original draft preparation, and writing—review and editing. S.K.: Conceptualization, formal analysis, funding acquisition, resources, supervision, and writing—review and editing. M.C.: Data curation, formal analysis, investigation, methodology, and writing—review and editing. R.R.: Conceptualization, funding acquisition, resources, supervision, and writing—review and editing. S.H.: Data curation, investigation, methodology, and writing—review and editing. V.N.: Writing—review and editing. D.M.: Conceptualization, funding acquisition, project administration, resources, supervision, and writing—review and editing. All authors have read and agreed to the published version of the article.

#### Author Disclosure Statement

The authors declare no conflict of interest. The funders had no role in the design of the study, in the collection,

analyses, or interpretation of data; in the writing of the article; or in the decision to publish the results.

#### Funding Information

The work has been performed within the laboratories of the Infrastructural Center of the University of Ljubljana, which is financially supported by the Slovenian Research Agency through infrastructural grant I0-0022. This work was supported by the Slovenian Research and Innovation Agency (ARIS) P2-0249, P2-0089, P3-0108, J2-3046, N2-0198, J2-60047, J2-3043, J3-3079, J7-4420. The authors acknowledge the CEMM Nanocenter (JSI, Slovenia) for the access to electron microscopy. This work has been also partly supported by the Research Council of Lithuania, Grant. Nr. S-MIP-23-124.

#### References

- Ginn SL, Amaya AK, Alexander IE, et al. Gene therapy clinical trials worldwide to 2017: An update. *J Gene Med* 2018;20(5):e3015–e3016; doi: 10.1002/jgm.3015
- Broderick KE, Chan A, Lin F, et al. Optimized in vivo transfer of small interfering RNA targeting dermal tissue using in vivo surface electroporation. *Mol Ther Nucleic Acids* 2012;1(2):e11; doi: 10.1038/mtna.2012.1
- Sachdev S, Potočnik T, Rems L, et al. Revisiting the role of pulsed electric fields in overcoming the barriers to in vivo gene electrotransfer. *Bioelectrochemistry* 2022;144:107994; doi: 10.1016/J.BIOELECTCHEM.2021.107994
- Rosazza C, Meglic HS, Zumbusch A, et al. Gene electrotransfer: A mechanistic perspective. *Curr Gene Ther* 2016; 16(2):98–129; doi: 10.2174/1566523216666160331130040
- Hernández JL, Coll T, Ciudad CJ. A highly efficient electroporation method for the transfection of endothelial cells. *Angiogenesis* 2004;7(3):235–241; doi: 10.1007/s10456-004-4180-8
- Mashel TV, Tarakanchikova YV, Muslimov AR, et al. Biomaterials Overcoming the delivery problem for therapeutic genome editing : Current status and perspective of non-viral methods. *Biomaterials* 2020;258(July):120282; doi: 10.1016/j.biomaterials.2020.120282

7. Geboers B, Scheffer HJ, Graybill PM, et al. High-Voltage electrical pulses in oncology: Irreversible electroporation, electrochemotherapy, gene electrotransfer, electrofusion, and electroimmunotherapy. *Radiology* 2020;295(2):254–272; doi: 10.1148/radiol.2020192190
8. Bradley CJ, Haines DE. Pulsed field ablation for pulmonary vein isolation in the treatment of atrial fibrillation. *J Cardiovasc Electrophysiol* 2020;31(8):2136–2147.
9. Chun K-RJ, Miklavčič D, Vlachos K, et al. State-of-the-Art pulsed field ablation for cardiac arrhythmias : Ongoing evolution and future perspective. *Europace* 2024;26(6):euae134; doi: 10.1093/europace/euae134
10. Mahnič-Kalamiza S, Miklavcic D. The Phenomenon of Electroporation. SpringerLink. 2022. Available from: [https://link.springer.com/chapter/10.1007/978-3-030-70586-2\\_3](https://link.springer.com/chapter/10.1007/978-3-030-70586-2_3) [Last accessed: May 27, 2025].
11. Novickij V, Dermol J, Grainys A, et al. Membrane permeabilization of mammalian cells using bursts of high magnetic field pulses. *PeerJ* 2017;5(April):e3267; doi: 10.7717/peerj.3267
12. Kranjc S, Kranjc M, Scancar J, et al. Electrochemotherapy by pulsed electromagnetic field treatment (PEMF) in mouse melanoma B16F10 in vivo. *Radiol Oncol* 2016;50(1):39–48; doi: 10.1515/raon-2016-0014
13. Novickij V, Kranjc M, Staigvila G, et al. High-Pulsed electromagnetic field generator for contactless permeabilization of cells in vitro. *IEEE Trans Magn* 2020;56(5):1–6; doi: 10.1109/TMAG.2020.2979120
14. Chen C, Evans JA, Robinson MP, et al. Electroporation of cells using EM induction of ac fields by a magnetic stimulator. *Phys Med Biol* 2010;55(4):1219–1229; doi: 10.1088/0031-9155/55/4/021
15. Kranjc Brezar S, Kranjc M, Čemažar M, et al. Electrotransfer of siRNA to silence enhanced green fluorescent protein in tumor mediated by a high intensity pulsed electromagnetic field. *Vaccines (Basel)* 2020;8(1):49; doi: 10.3390/vaccines8010049
16. Miklavcic D, Novickij V, Kranjc M, et al. Contactless electroporation induced by high intensity pulsed electromagnetic fields via distributed nanoelectrodes. *Bioelectrochemistry* 2020;132:107440; doi: 10.1016/j.bioelechem.2019.107440
17. Kranjc M, Dermol-Černe J, Potočnik T, et al. High-Intensity pulsed electromagnetic field-mediated gene electrotransfection in vitro. *Int J Mol Sci* 2022;23(17):9543; doi: 10.3390/ijms23179543
18. Goršak T, Drab M, Krizaj D, et al. Magneto-mechanical actuation of barium-hexaferite nanoplatelets for the disruption of phospholipid membranes. *J Colloid Interface Sci* 2020;579:508–519; doi: 10.1016/j.jcis.2020.06.079
19. Ghorbel A, André FM, Mir LM, et al. Electrophoresis-assisted accumulation of conductive nanoparticles for the enhancement of cell electroporation. *Bioelectrochemistry* 2021;137:107642; doi: 10.1016/j.bioelechem.2020.107642
20. Rolong A, Prokop KJ, Davalos RV. Impact of the use of nanoparticles on electric field distribution during irreversible electroporation treatments: Can the lesion be enhanced beyond IRE margin? In: *IFMBE Proceedings* 2015:793–796; doi: 10.1007/978-3-319-11128-5\_197
21. Raffa V, Riggio C, Smith MW, et al. BNNT-Mediated irreversible electroporation: Its potential on cancer cells. *Technol Cancer Res Treat* 2012;11(5):459–465; doi: 10.7785/tcrt.2012.500258
22. Zu Y, Huang S, Liao WC, et al. Gold nanoparticles enhanced electroporation for mammalian cell transfection. *J Biomed Nanotechnol* 2014;10(6):982–992; doi: 10.1166/jbn.2014.1797
23. Ghorbel A, Mir LM, García-Sánchez T. Conductive nanoparticles improve cell electroporation. *Nanotechnology* 2019;30(49):495101; doi: 10.1088/1361-6528/ab3be9
24. Rezaee Z, Yadollahpour A, Bayati V, et al. Gold nanoparticles and electroporation impose both separate and synergistic radiosensitizing effects in HT-29 tumor cells: An in vitro study. *Int J Nanomedicine* 2017;12:1431–1439; doi: 10.2147/IJN.S128996
25. Nikoobakht B, El-Sayed MA. Preparation and growth mechanism of Gold Nanorods (NRs) using seed-mediated growth method. *Chem Mater* 2003;15(10):1957–1962; doi: 10.1021/cm0207321
26. Liu K, Zheng Y, Lu X, et al. Biocompatible gold nanorods: One-Step surface functionalization, highly colloidal stability, and low cytotoxicity. *Langmuir* 2015;31(17):4973–4980; doi: 10.1021/acs.langmuir.5b00666
27. Ojea-Jiménez I, Bastús NG, Puentes V. Influence of the sequence of the reagents addition in the citrate-mediated synthesis of gold nanoparticles. *J Phys Chem C* 2011;115(32):15752–15757; doi: 10.1021/jp2017242
28. Bastús NG, Comenge J, Puentes V. Kinetically controlled seeded growth synthesis of citrate-stabilized gold nanoparticles of up to 200 nm: Size focusing versus ostwald ripening. *Langmuir* 2011;27(17):11098–11105; doi: 10.1021/la201938u
29. Stöber W, Fink A, Bohn E. Controlled growth of monodisperse silica spheres in the micron size range. *J Colloid Interface Sci* 1968;26(1):62–69; doi: 10.1016/0021-9797(68)90272-5
30. Hanahan D, Weinberg RA. Hallmarks of cancer: The next generation. *Cell* 2011;144(5):646–674; doi: 10.1016/j.cell.2011.02.013
31. Dermol J, Pakhomova ON, Pakhomov AG, et al. Cell electrosensitization exists only in certain electroporation buffers. *PLoS One* 2016;11(7):e0159434; doi: 10.1371/journal.pone.0159434
32. Polajžer T, Dermol-Černe J, Reberšek M, et al. Cancellation effect is present in high-frequency reversible and irreversible electroporation. *Bioelectrochemistry* 2020;132:107442; doi: 10.1016/J.BIOELECTROCHEM.2019.107442
33. Polajžer T, Kranjc M, Kralj S, et al. Limited efficacy of nanoparticle-assisted electroporation for membrane permeabilization and gene electrotransfer. *Pharmaceutics* 2025;17(8):964; doi: 10.3390/pharmaceutics17080964
34. Franco-Ulloa S, Tatulli G, Bore SL, et al. Dispersion state phase diagram of citrate-coated metallic nanoparticles in saline solutions. *Nat Commun* 2020;11(1):5422; doi: 10.1038/s41467-020-19164-3
35. Park J-W, Shumaker-Parry JS. Structural study of citrate layers on gold nanoparticles: Role of intermolecular interactions in stabilizing nanoparticles. *J Am Chem Soc* 2014;136(5):1907–1921; doi: 10.1021/ja4097384
36. Wu X, Dai H, Liu L, et al. Citrate reduced oxidative damage in stem cells by regulating cellular redox signaling pathways and represent a potential treatment for oxidative stress-

- induced diseases. *Redox Biol* 2019;21:101057; doi: 10.1016/j.redox.2018.11.015
37. Caiazza C, D'Agostino M, Passaro F, et al. Effects of long-term citrate treatment in the PC3 prostate cancer cell line. *Int J Mol Sci* 2019;20(11):2613; doi: 10.3390/ijms20112613
38. von Schirnding C, Giopanou I, Hermawan A, et al. Synergistic combination of calcium and citrate in mesoporous nanoparticles targets pleural tumors. *Chem* 2021;7(2):480–494; doi: 10.1016/j.chempr.2020.11.021
39. Costello LC, Franklin RB. The implications of the hypocitricemic response to surgery and the role of liver function and hepatocyte metabolism: An important, but neglected, clinical relationship. *J Liver Res Disord Ther* 2018;4(3):114–119; doi: 10.15406/jlrtd.2018.04.00112
40. Suk JS, Xu Q, Kim N, et al. PEGylation as a strategy for improving nanoparticle-based drug and gene delivery. *Adv Drug Deliv Rev* 2016;99(Pt A):28–51; doi: 10.1016/j.addr.2015.09.012
41. Rosazza C, Deschout H, Buntz A, et al. Endocytosis and endosomal trafficking of DNA after gene electrotransfer in vitro. *Mol Ther Nucleic Acids* 2016;5(2):e286; doi: 10.1038/mtna.2015.59
42. Wu M, Yuan F. Membrane binding of plasmid DNA and endocytic pathways are involved in electrotransfection of mammalian cells. *PLoS One* 2011;6(6):e20923; doi: 10.1371/journal.pone.0020923
43. Potočnik T, Sachdev S, Polajžer T, et al. Efficient gene transfection by electroporation—In vitro and in silico study of pulse parameters. *Appl Sci* 2022;12(16):8237; doi: 10.3390/app12168237

Address correspondence to:

*Damijan Miklavčič, PhD*  
*Faculty of Electrical Engineering*  
*University of Ljubljana*  
*Tržaška cesta 25*  
*Ljubljana 1000*  
*Slovenia*

*E-mail: damijan.miklavcic@fe.uni-lj.si*